Available online at www.sciencedirect.com

ScienceDirect

Procedia Engineering 82 (2014) 127 – 135

Procedia Engineering

www.elsevier.com/locate/procedia

23rd International Meshing Roundtable (IMR23)

A thermo-elastic analogy for high-order curvilinear meshing with control of mesh validity and quality

D. Moxey[a,*], D. Ekelschot[a], Ü. Keskin[a], S. J. Sherwin[a], J. Peiró[a]

[a]*Department of Aeronautics, Imperial College London, London, SW7 2AZ, UK.*

Abstract

In recent years, techniques for the generation of high-order curvilinear mesh have frequently adopted mesh deformation procedures to project the curvature of the surface onto the mesh, thereby introducing curvature into the interior of the domain and lessening the occurrence of self-intersecting elements. In this article, we propose an extension of this approach whereby thermal stress terms are incorporated into the state equation to provide control on the validity and quality of the mesh, thereby adding an extra degree of robustness which is lacking in current approaches.

Peer-review under responsibility of organizing committee of the 23rd International Meshing Roundtable (IMR23)

Keywords:

1. Introduction

Mesh deformation techniques change the position of nodes in the mesh without changing the underlying connectivity. They are used, amongst other purposes, to improve the quality of a mesh of linear elements, to incorporate boundary layer meshes into an existing mesh and to generate curved high-order elements. Some of the most popular methods are, for instance, Laplacian smoothing [2,8], Winslow smoothing [9,10], elastic mesh deformation [3,10,13] and mesh optimisation [1,4,6]. The focus here is in the use of elastic mesh deformation techniques for the generation of boundary-conforming high-order curvilinear meshes. Previous work in this area using either linear [3,14] or non-linear elasticity [7] lacks mechanisms for controlling the validity and quality of the deformed mesh.

Here we propose a method that incorporates additional terms in the linear elasticity equations that can be interpreted as thermal stresses and that aim to counteract distortion generated by the imposed displacement at the boundary. Making the thermal stresses dependent on measures of mesh quality for high-order elements will permit us to control the validity and quality of the mesh. A precursor to this idea was presented in the work by Palmerio [8] for linear elements where a pseudo-pressure term was used to ensure the area of the elements in the mesh remained positive through the smoothing process. The penalty term proposed in [8] can be seen as a particular case of the linear isotropic thermal stresses in the current formulation. Our formulation is however more general; it provides a physical

* Corresponding author. Tel.: +0-000-000-0000 ; fax: +0-000-000-0000.
E-mail address: d.moxey@imperial.ac.uk

Peer-review under responsibility of organizing committee of the 23rd International Meshing Roundtable (IMR23)
doi:10.1016/j.proeng.2014.10.378

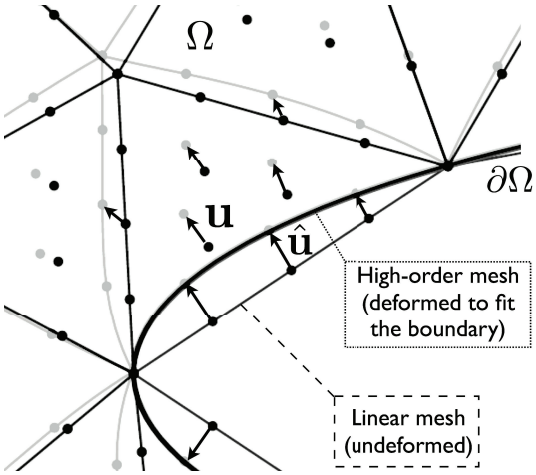

Fig. 1. Mesh deformation driven by boundary displacement.

interpretation of the additional terms that control mesh validity and quality, and it can be generalized to account for mesh anisotropy.

We begin by describing the governing equations of elasticity, which incorporates body forces and thermal stresses in section 2, and outline its numerical discretization using spectral/*hp* elements in section 3. Section 5 proposes some example forms of the tensor of thermal stresses and illustrates with a practical example that the modifications to the elasticity equations proposed here permit a higher degree of deformation whilst maintaining the validity of the underlying high-order elements.

2. Mesh deformation via linear elasticity

We seek to deform a mesh of straight-sided high-order elements to accommodate curved boundaries. To achieve this, we adopt a linear elasticity formulation in terms of the displacement, $\mathbf{u}$, of points in the domain, $\Omega \subset \mathbb{R}^n$, caused by imposing a prescribed displacement, $\hat{\mathbf{u}}$, at the points in the boundary of the domain, $\partial\Omega$. This is illustrated in Fig. 1.

The elastic formulation starts with the equilibrium of forces represented by the equation

$$\nabla \cdot \mathbf{S} + \mathbf{f} = \mathbf{0} \quad \text{in} \quad \Omega \tag{1}$$

where $\mathbf{S}$ is the stress tensor and $\mathbf{f}$ denotes a distributed force. The force will be, in general, a function of the position, i.e. $\mathbf{f}(\mathbf{x})$ with $\mathbf{x} \in \mathbb{R}^n$.

We further assume that the stress tensor $\mathbf{S}$ incorporates both elastic and thermal stresses, so that it can be written as

$$\mathbf{S} = \mathbf{S}_e + \mathbf{S}_t,$$

where the subscripts e and t denote the elastic and thermal terms respectively.

We adopt the usual linear form of the elastic stress tensor as

$$\mathbf{S}_e = \lambda \,\mathrm{Tr}(\mathbf{E})\,\mathbf{I} + \mu\mathbf{E},$$

where λ and μ are the Lamé constants, $\mathbf{E}$ represents the strain tensor, and $\mathbf{I}$ is the identity tensor. For small deformations, the strain tensor $\mathbf{E}$ is given as

$$\mathbf{E} = \frac{1}{2}\left(\nabla\mathbf{u} + \nabla\mathbf{u}^t\right). \tag{2}$$

The boundary conditions required to close the problem consist of prescribed displacements at the boundary $\partial\Omega$, i.e.

$$\mathbf{u} = \hat{\mathbf{u}} \quad \text{in } \partial\Omega. \tag{3}$$

We further express the Lamé constants in terms of the Young's modulus E and Poisson ratio ν as

$$\lambda = \frac{\nu E}{(1+\nu)(1-2\nu)}, \qquad \mu = \frac{E}{2(1+\nu)}.$$

Note that the elastic parameters of the problem λ and μ, or equivalently E and ν, might be considered to be functions of $\mathbf{x}$. This is a strategy used for instance in reference [13] where smaller elements are made stiffer to permit larger deformations.

The simplest model of thermal stresses is that of a linear isotropic material and the corresponding thermal stress tensor is of the form

$$\mathbf{S}_t = \beta(T - T_0)\mathbf{I}$$

where T is the temperature, T_0 is the temperature of the stress-free state, and β is a thermal coefficient. We will consider the temperature to be a function of the position, i.e. $T(\mathbf{x})$.

The main idea of the paper is to use this term to control the validity of the mesh and its quality. If the displacement of the boundary nodes is causing an element to distort, we could increase or decrease the temperature to locally expand or contract, respectively, the element so as to prevent the element becoming invalid. We will discuss some potential forms of the thermal stresses for the purpose of controlling mesh validity and quality in section 5, but we assume that they do not depend on $\mathbf{u}$.

3. Implementation within Nektar++

To obtain a spectral/hp element discretisation of this problem, we select a mesh of the domain $\Omega = \bigcup_{e=1}^{N_{\text{el}}} \Omega^e$ and sets of trial and test spaces of continuous functions

$$\mathcal{X} = \{\mathbf{v} \in C^0(\Omega) \mid \mathbf{v}|_{\Omega^e} \in [\mathcal{P}_N(\Omega^e)]^n, \mathbf{v}|_{\partial\Omega} = \hat{\mathbf{u}}\},$$
$$\mathcal{V} = \{\mathbf{v} \in C^0(\Omega) \mid \mathbf{v}|_{\Omega^e} \in [\mathcal{P}_N(\Omega^e)]^n, \mathbf{v}|_{\partial\Omega} = 0\},$$

where $\mathcal{P}_N(\Omega^e)$ is the space of all polynomials of degree up to N. Multiplying (1) by a test function $\mathbf{v} \in \mathcal{V}$, taking an approximate solution $\mathbf{u}^h \in \mathcal{X}$ and integrating by parts, we obtain the weak formulation: find $\mathbf{u}^h \in \mathcal{X}$ such that

$$\int_\Omega \nabla\mathbf{v} : \mathbf{S}(\mathbf{u}^h)\, dx = -\int_\Omega \mathbf{f}\,\mathbf{v}\, dx \tag{4}$$

for all $\mathbf{v} \in \mathcal{V}$. The discretisation of this system is performed using the spectral/hp element framework described in [5] and implemented in the open-source code `Nektar++` [11], which supports elements such as triangles and tetrahedra as well as quadrilateral, prismatic, pyramidal and hexahedral elements, and the various hybrid meshes which can be obtained by connecting them, through the use of a set of hierarchical C^0 tensor product modal basis functions.

To facilitate the use of numerical integration required for the calculation of the integrals in the discrete system (4), a high-order element, denoted by Ω^e, is represented as the image of a standard or reference element, Ω_{st}, by a mapping $\mathcal{M}$. This is depicted in Fig. 2 for a high-order triangular element.

The mapping plays an important role in the quality of the mesh and the conditioning of the system of equations (4). The Jacobian matrix of the mapping $\mathbf{J}$, its determinant J (hereafter referred to as the Jacobian) and the metric tensor, $\mathbf{G} = \mathbf{J}^t\mathbf{J}$ provide measures of distortion of the physical element, with respect to the reference element, that can be used to determine the validity of the element and used to assess its quality. For instance, the Jacobian locally relates areas in the reference and physical elements and a value $J \leq 0$ indicates that the element is inverted with negative or zero area and thus it is invalid for computation unless specific measures are taken to account for this, as outlined in e.g. [12]. On the other hand, the metric tensor contains directional information that allows us to account for anisotropy in elemental distortion.

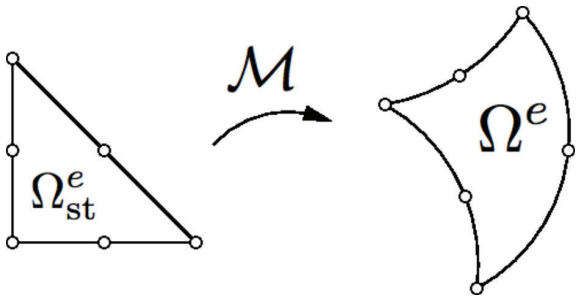

Fig. 2. Representation of a triangular high-order element as a mapping, $\mathcal{M} : \Omega^e_{\mathrm{st}} \to \Omega^e$, where Ω^e_{st} is a reference element and Ω^e is the physical element. Other elemental shapes are represented in a similar fashion.

In this discretisation, the thermal stress terms are not a function of $\mathbf{u}$ and so can be omitted from the stiffness matrix arising from the elastic stress tensor $\mathbf{S}_e$. For small problems, the matrix system described by the left hand side of (4) is globally assembled across all elements, and the solution found with a direct Cholesky decomposition. For larger problems, particularly in three dimensions, we construct a matrix representation of $\mathbf{S}_e$ on each element and utilise a Jacobi-preconditioned conjugate gradient method within `Nektar++` to invert the system across multiple processors. Optionally, a statically condensed system on which we solve for only the degrees of freedom lying on the boundary of each element can be constructed, which gives significant efficiency improvements at high polynomial orders. To give an indication of performance, each step (including matrix generation and linear solve) for a 1000 element triangular mesh at polynomial order $P = 6$ requires around 1.5 seconds of runtime on a single core of a Intel Xeon E5-2690 processor. It should be noted however that no particular efforts have been made to optimise these routines (especially in regards to matrix generation).

4. Application to mesh generation

In figure 3 we demonstrate the general methodology of the linear elastic analogy used in the coming results when applied to a mesh generation problem. The starting point is a small boundary layer grid of 72 triangular elements, on which we intend to apply a large sinusoidal deformation to the bottom edge. Since the linear elastic equations are only valid when small deformations are considered, we choose to adopt a sub-stepping approach, whereby the large deformation at the boundary is split into a number of smaller steps in order to allow the generation of a valid mesh. At the end of each step, we apply the deformation to the mesh, reconstruct the matrix system on the grid to account for the updated geometric factors and then solve the linear system to obtain the next solution field. In the example of figure 3 we have used 100 steps to achieve the deformation of the boundary.

Here, and in all the examples that follow, we have assumed $\mathbf{f} = \mathbf{0}$ and constant values of the elastic parameters E and ν. In the absence of a source term, the value of Young's modulus, E, is not important since it is just a multiplicative factor in the expression of the stresses. On the other hand, the Poisson ratio, ν, is a measure of the compressibility of the material and it is chosen as the maximum value in its allowable range, $0 < \nu < \frac{1}{2}$, that would permit to accommodate the area changes induced by the displacement of the boundary. We have used $\nu = 0.3$ in the present case.

5. Effect of thermal stresses

To illustrate the effect of the additional thermal stresses in the validity and quality of the mesh we use a simple geometry that consists of a square plate $[-1, 1]^2$ with circular hole of radius $r = 0.1$ which is depicted in Fig. 4. The points in the boundary of the circular hole are rotated about its center by an angle θ and are kept stationary at the boundary of the square. Our objective is to determine the maximum value $\theta_{\max}$ of the angle that we can impose before the appearance of the first invalid element, i.e. one with a zero or negative Jacobian. Given that we are solving the

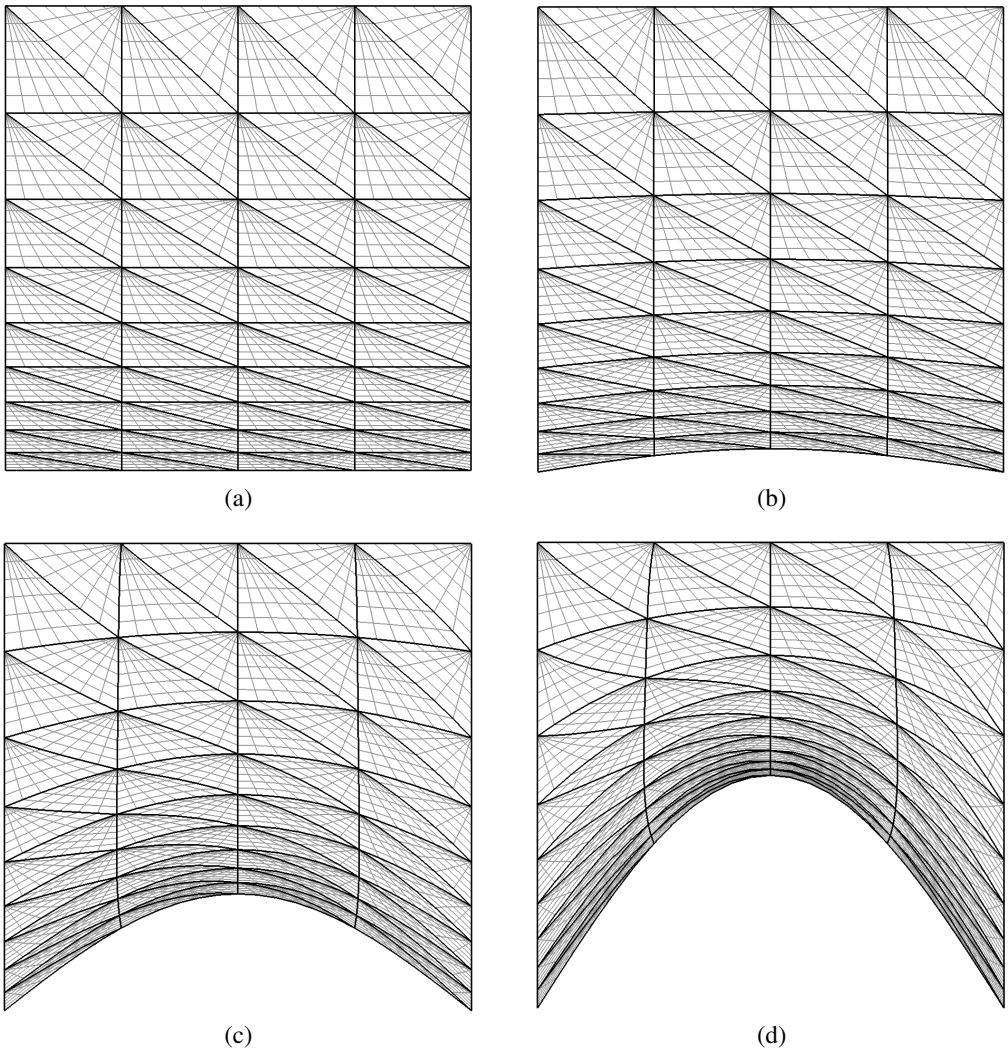

Fig. 3. Application of the mesh deformation analogy to a prototype boundary layer mesh. The high order elements are highlighted with dark lines, and interior quadrature points with light lines. (a) Original linear grid; (b) deformation after 10 steps; (c) 50 steps; (d) final deformed grid at 100 steps.

linear elasticity equations which are only valid for small deformations, the rotation is applied in small angular steps $\Delta\theta = 1^\circ$.

We consider two formulations to control mesh quality through the thermal stresses: an isotropic one based on the Jacobian of the elemental mapping and an anisotropic one that utilises the eigenvalues of the metric tensor of the mapping to account for anisotropy in the deformation of the mesh.

5.1. Isotropic case

Here we consider an isotropic tensor of thermal stresses of the form

$$\mathbf{S}_t = \beta J \mathbf{I} \tag{5}$$

where J is the Jacobian of the elemental mapping of the element, β is a scaling factor and $\mathbf{I}$ is the identity tensor.

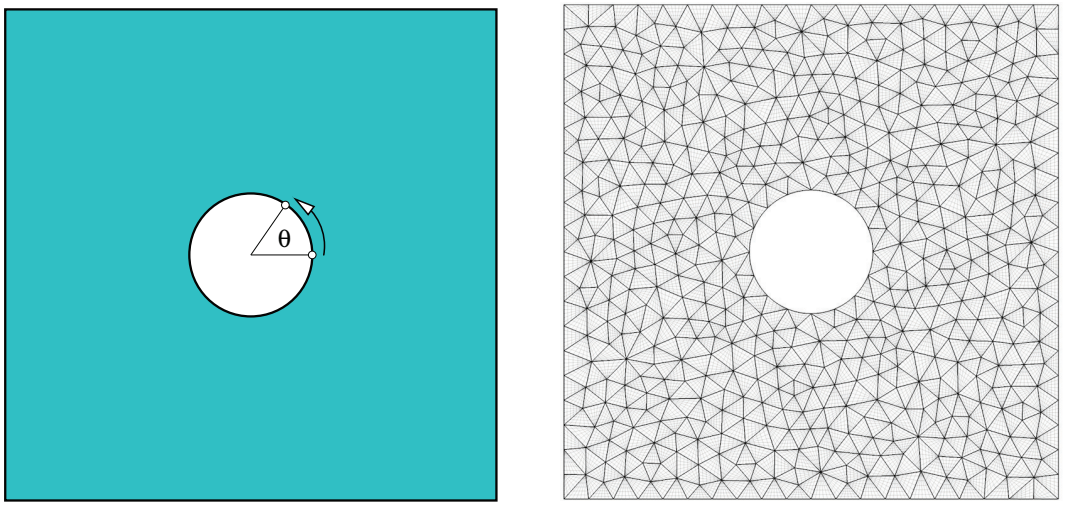

Fig. 4. Test case used to illustrate the effect of thermal stresses: (a) The computational domain is a square plate with circular holes and the points in the circle are rotated about its center by an angle θ; (b) Initial mesh consisting of 1031 high-order triangles (thicker outline) with interior points shown (thin outline).

In the test case we rotate the circular hole by small angular steps to reach an angle θ and determine the maximum angle $\theta_{\max}$ than can be reached before an element becomes invalid with $J \leq 0$. The value of $\theta_{\max}$ as a function of β is shown in Fig. 5(a). We also consider three polynomial orders $P = 3, 6, 9$ to demonstrate how thermal stresses affect both high- and low-order element types.

The value $\beta = 0$ corresponds to the absence of thermal terms for which $\theta_{\max} \approx 80^\circ$ almost independently of the polynomial order. The inclusion of thermal stresses clearly improves the performance of the mesh deformation algorithm. It allows higher values of $\theta_{\max}$ for $\beta > 0$ and the best values for $\theta_{\max}$ are obtained in the approximate range $20 \leq \beta \leq 25$ with corresponding best values of maximum angle in the range $120^\circ \leq \beta_{\max} \leq 130^\circ$ which is a significant improvement with respect to the non-heated case. The deformed mesh and iso-contours of temperature for $\theta_{\max} = 130^\circ$ in the case where $P = 6$ are shown in Fig. 5(b).

To measure the effect of the isotropic temperature terms on the solution field, for each element we calculate the scaled Jacobian

$$J_s = \frac{\min J(\xi)}{\max J(\xi)},$$

a straightforward measure of quality which is one for all straight sided elements. Whilst this measure of quality is not necessarily ideal in all circumstances, for this application we note that values of J_s which differ significantly from one indicate badly conditioned elements. We measure the distribution of the scaled Jacobians in the mesh at a fixed rotation angle of 75°. Figure 6 shows the difference in distributions when no thermal stresses are used and when the isotropic thermal stress is applied with $\beta = 25$ at $P = 6$. We clearly see that the thermal stress has a positive impact on the quality of the elements, with the entire distribution shifting to the right and the lowest value of the scaled Jacobian significantly increased, demonstrating a notable improvement in the quality of the elements at this rotation angle.

5.2. Anisotropic case

The thermal stress term proposed in this section is based on an eigenvalue decomposition of the metric tensor, $\mathbf{G}$, of the elemental mapping $\mathcal{M}$. It is represented by a $n \times n$ matrix with n being the spatial dimension and can be expressed as

$$\mathbf{G} = \mathbf{V}\mathbf{D}\mathbf{V}^{-1} \tag{6}$$

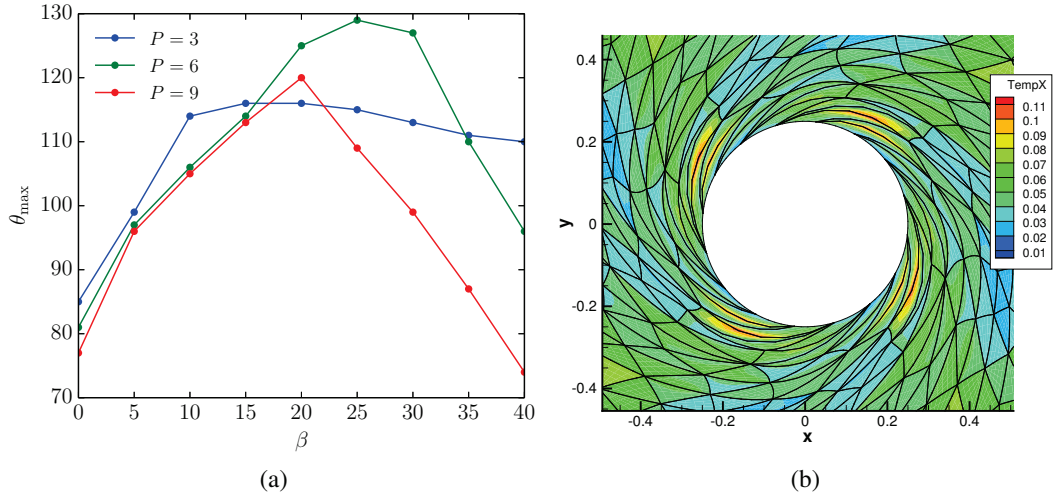

Fig. 5. Isotropic thermal stresses: (a) The maximum rotation angle $\theta_{\max}$ as a function of the scaling coefficient β for polynomial orders $P = 3, 6, 9$; (b) Enlargement near the circular hole of the mesh and iso-contours of thermal stresses at $\theta_{\max}$ for $P = 6$.

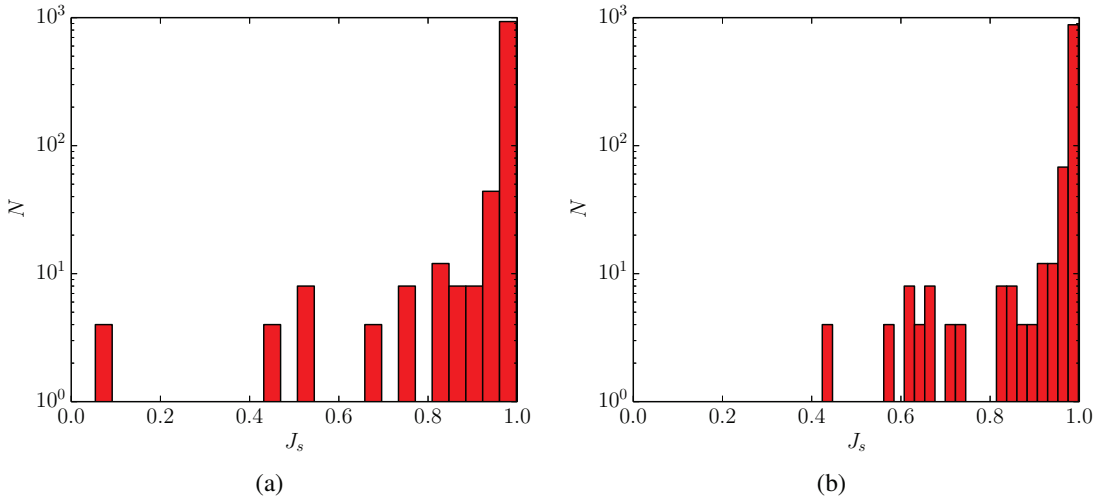

Fig. 6. Histograms showing the number of elements N with scaled Jacobian J_s after a rotation of 75° at polynomial order $P = 6$ and $\beta = 25$. (a) No temperature term; (b) with isotropic thermal stresses.

where $\mathbf{V}$ is the matrix of the eigenvectors of $\mathbf{G}$ and $\mathbf{D}$ is a diagonal matrix whose entries are the corresponding eigenvalues. The eigenvalues of the metric tensor give a measure of distortion in the direction of its eigenvectors. We take advantage of this property to construct the anisotropic thermal as

$$\mathbf{S}_t = \beta J \mathbf{V}\hat{\mathbf{D}}\mathbf{V}^{-1} \tag{7}$$

where $\hat{\mathbf{D}}$ is a diagonal matrix. Its entries are obtained by suitably scaling the eigenvalues of $\mathbf{D}$ to counteract the elemental distortion generated by the displacement of the boundary.

Fig. 7 shows the maximum angle obtained for our test case for various values of β. The maximum angle is always higher than in the non-thermal case ($\beta = 0$) and there is an optimal value of $\beta \approx 250$ for all the polynomial orders

($P = 3, 6, 8$) leading to a best value $\theta_{\max} = 115°$. The value of $\theta_{\max}$ is more sensitive to the polynomial order than in the isotropic case. The best value of $\theta_{\max}$ is slightly smaller than the one obtained in the previous case but leads to smaller values of the gradient of thermal stresses as shown in Fig. 8.

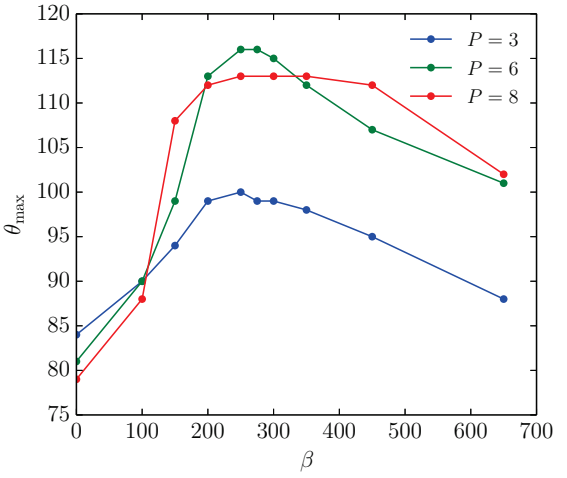

Fig. 7. The maximum rotation angle $\theta_{\max}$ shown as a function of the scaling coefficient β for the case of anisotropic thermal stresses and polynomial orders $P = 3, 6, 8$.

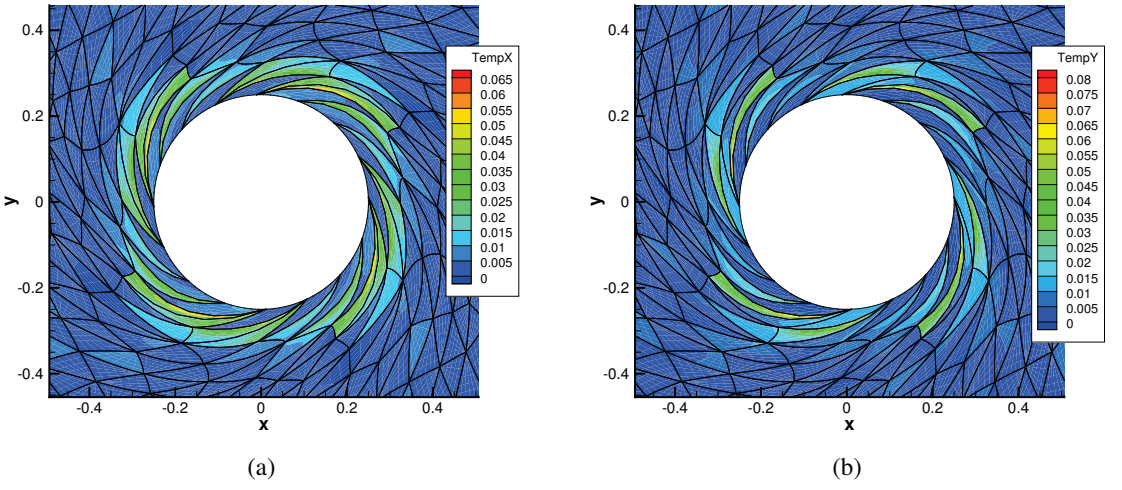

Fig. 8. Mesh and iso-contours of $\mathbf{T} = \nabla \cdot \mathbf{S} = (T_x, T_y)$ for the case of anisotropic thermal stresses corresponding to maximum allowable distortion at $\theta_{\max}$ and $P = 6$: (a) T_x ; (b) T_y.

6. Conclusions

We have shown that incorporating thermal stresses which depend on quantities representative of the distortion of the element, such as the Jacobian and the metric tensor of the mapping, permits controlling the quality of high-order

meshes generated by deforming a linear mesh through the displacement of its boundary nodes. A simple example of a rotating circular hole on a square plate has illustrated that the proposed methodology allows for higher distortions than the one based on elastic stresses only. This work is a two-dimensional proof-of-concept that is amenable to straightforward extension to three-dimensional problems. Further control on the mesh quality can be achieved by the implementation of more sophisticated measures of high-order mesh quality that are less sensitive to the shape of the reference element.

References

[1] A. Gargallo-Peiró, X. Roca, J. Peraire and J. Sarrate. Defining quality measures for validation and generation of high-order tetrahedral meshes. In *22nd International Meshing Roundtable*, pages 109–126, Orlando, Florida, October 2014. Springer-Verlag.

[2] G. Hansen and A. Zardecki and D. Greening and R. Bos. A finite element method for three-dimensional unstructured grid smoothing. *Journal of Computational Physics*, 202:281–297, 2005.

[3] R. Hartmann, J. Held, T. Leicht, and F. Prill. Discontinuous Galerkin methods for computational aerodynamics 3D adaptive flow simulation with the DLR PADGE code. *Aerospace Science and Technology*, 14:512–519, 2010.

[4] J-F. Remacle and T. Toulorge and J. Lambrechts. Robust untangling of curvilinear meshes. *Proceedings of the 21st International Meshing Roundtable*, pages 71–83, 2013.

[5] G.E. Karniadakis and S.J. Sherwin. *Spectral/hp Element Methods for Computational Fluid Dynamics*. Oxford University Press, second edition, 2005.

[6] L.A. Freitag and P.M. Knupp. Tetrahedral mesh improvement via optimization of the element condition number. *Int. J. Num. Meth. Eng.*, 53:1377–1391, 2002.

[7] P. Persson and J. Peraire. Curved mesh generation and mesh refinement using Lagrangian solid mechanics. In *Proceedings of the 47th Aerospace Sciences Meeting and Exhibit*, number AIAA 2009-949, Orlando, Florida, USA, January 2009. AIAA.

[8] B. Palmerio. An attraction-repulsion mesh adaption model for flow solution on unstructured grids. *Computers Fluids*, 23(3):487–506, 1994.

[9] P.M. Knupp. Winslow smoothing on two-dimensional unstructured meshes. *Engineering with Computers*, 15(3):263–268, 1999.

[10] S. L. Karman. Unstructured viscous layer insertion using linear-elastic smoothing. *AIAA*, 45(1):168–180, January 2007.

[11] S.J. Sherwin and R.M. Kirby. `www.nektar.info`.

[12] S.M. Shontz and S.A. Vavasis. Analysis of and workarounds for element reversal for a finite element-based algorithm for warping triangular and tetrahedral meshes. *BIT Numer. Math.*, 50:863–884, 2010.

[13] K. Stein, T. Tezduyar, and R. Benney. Mesh moving techniques for fluid-structure interactions with large displacements. *ASME J. Appl. Mech.*, 70:5863, 2003.

[14] Z.Q. Xie and R. Sevilla and O. Hassan and K. Morgan. The generation of arbitrary order curved meshes for 3D finite element analysis. *Comput Mech.*, 51:361–374, 2013.